Neutral Lipophilic Palladium(II) Complexes and their Applications in Electrocatalytic Hydrogen Production and C-C Coupling Reactions

Olesea Cuzan-Munteanu,[b,c] Dumitru Sirbu,[a] Michel Giorgi,[d] Sergiu Shova,[e] Elizabeth A. Gibson,[a] Marius Réglier,[c] Maylis Orio,[c] Luísa M. D. R. S. Martins,[f] and Andrew C. Benniston[a]

This work is dedicated to the memory of Prof. Constantin Turta for his outstanding contribution to the field of inorganic chemistry.

Abstract: Three neutral palladium(II) complexes [Pd$(L_n)_2$] (n = 1,2,3) containing benzotriazole-phenolate ligands **HL_1** = 2-(2H-benzotriazol-2-yl)-6-dodecyl-4-methylphenol; **HL_2** = 2-(2H-benzotriazol-2-yl)-4,6-di-tert-pentylphenol; **HL_3** = 2-(2H-benzotriazol-2-yl)-4,6-bis(1-methyl-1-phenylethyl)phenol were synthesized and characterized by several spectroscopic methods (^{1}H, ^{13}C NMR, UV-Visible), ESI mass spectrometry and single-crystal X-ray diffraction. The geometry around the palladium(II) center for each complex is described as distorted square planar. The complexes were tested as potential catalysts for electrochemical proton reduction in DMF using trifluoracetic acid (TFA). Gas analysis under electrocatalytic conditions at a boron-doped diamond working electrode confirmed the hydrogen production. After performing similar gas analysis experiments using a working mercury pool electrode, no hydrogen was detected which supports the concept that the active species of the catalytic process are palladium particles formed on the surface of the working electrode. The palladium(II) benzotriazolyl phenolate complexes facilitate the formation of particles for electrocatalytic hydrogen production. Furthermore, the palladium(II) complexes **PdL_2** and **PdL_3** were able to catalyze microwave-assisted Heck and Sonogashira C-C coupling reactions.

[a] Prof A C Benniston, Dr E Gibson, Dr D Sirbu,
Chemistry-School of Natural & Environmental Sciences
Newcastle University
Newcastle upon Tyne, NE1 7RU, UK
E-mail: andrew.benniston@ncl.ac.uk
[b] Dr O Cuzan-Munteanu
Institute of Chemistry
3 Academiei Street
Chisinau MD-2028, Moldova
[c] Prof M Réglier, Dr M Orio, Dr O Cuzan-Munteanu
Aix Marseille Université
Centrale Marseille, CNRS, ISM2 UMR 7313,
Marseille 13397, France
[d] Dr M Giorgi
Aix Marseille Université
CNRS, Centrale Marseille, FSCM, Spectropole, Marseille, France
[e] Dr S Shova
Institute of Macromolecular Chemistry "Petru Poni", Department of Inorganic Polymers,
41A Grigore Ghica Voda Alley,
Iasi-700487, Romania
[f] Prof L M D R S Martins
Centro de Química Estrutural,
Instituto Superior Técnico, Universidade de Lisboa, Av. Rovisco Pais, 1049-001
E-mail: luisammartins@tecnico.ulisboa.pt

Introduction

Palladium chemistry is a highly investigated field of study and is the basis for many industrially important processes.[1] The oxidative activity of palladium-based catalysts is one main dynamic area of investigation,[2] and several groups are interested not only in the catalytic activity of palladium complexes, but also in the reaction mechanism, isolation of intermediates and characterization of different redox-active species.[3] Another pertinent feature of palladium is its ability when complexed to perform reductive-based reactions thus making it a truly versatile metal. Focusing in the first instance on reductive chemistry, palladium and its complexes are considered to be good catalysts for hydrogen evolution reaction,[4] though there is still much scope for improvement especially in the area of electrocatalytic hydrogen generation from protons. The dinuclear palladium(I)1,3-bis[(2-chloro)benzene]triazenide complex,[5] for instance, was shown to produce hydrogen from acetic acid in dichloromethane (DCM), based on cyclic voltammetry experiments, but no detection of the electrolysis product was performed. The palladium(II) meso-tetraferrocenylporphyrine[6] also showed some promising results for electrocatalytic H_2 production and in this case the product could be identified. A faradaic efficiency of 70% was obtained for proton reduction in dimethylformamide (DMF) at -1.5 V *vs*. saturated calomel electrode (SCE) at a glassy carbon working electrode. A mononuclear palladium complex based on a thiosemicarbazone ligand[7] has shown electrocatalytic behaviour for proton reduction in DMF in the presence of TFA, however the faradaic efficiency of this compound was only 34% with a turnover number of 2 after 4h.

The reductive carbon-carbon bond forming capabilities of *in-situ* palladium species is dominated by coupling reactions such as Suzuki,[8] Sonagashira,[9] Heck[10] and Negishi,[11] relying in many cases on the production of zero-valent palladium in the first instance. The coordination sphere of the palladium is provided by ligands generally comprising soft donor atoms such a phosphorus (e.g., PPh_3), but other donor atoms have found application. For example, the 1,2,4-triazole-based palladium complex PdI[η^3-(C_6H_3-2,6-$(CH_2Tz)_2$)-*N*,*C*,*N*][10] was successfully tested as catalyst for the Heck coupling reaction. Another palladium complex derived from a 1,2,4-triazolin-5-ylidene containing ligand which coordinates through the CNC atoms[9]

has shown good catalytic performance in Sonogashira coupling with a turnover number of 8000. Also noted is the recently reported series of palladium(II) complexes with 3-(2-pyridyl)-5R-1,2,4-triazoles, where R = ethyl, *n*-propyl, *i*-propyl and *t*-butyl,[8] which are capable to catalyse the microwave-assisted Suzuki–Miyaura cross-coupling reaction in the presence of base.

As a follow up to our own work,[6,12] the focus was to develop palladium(II) coordinately unsaturated complexes based on robust and readily accessible ligands. A compound based upon the triazole-phenol moiety (Figure 1) offers a bidentate binding motif, and when deprotonated and complexed to palladium(II) in a 2:1 ratio forms a neutral complex. To increase solubility in common organic solvents the phenol group is a suitable unit to incorporate lipophilic alkyl groups. The three complexes (**PdL$_1$**-**PdL$_3$**) which were developed are promising for the electrocatalytic proton reduction into hydrogen and for Sonogashira and Heck C-C bond formation.

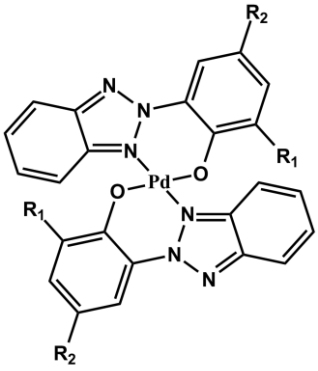

PdL$_1$ R_1 = dodecyl; R_2=methyl
PdL$_2$ $R_1 = R_2$ = *tert*-pentyl
PdL$_3$ $R_1 = R_2$ = 1-methyl-1-phenylethyl

Figure 1. Representation of the palladium(II) complexes discussed in the text and their nomenclature.

Results and Discussion

Synthesis and characterization

The commercially available compounds 2-(2H-benzotriazol-2-yl)-4,6-di-tert-pentylphenol (**HL$_2$**) and 2-(2H-benzotriazol-2-yl)-4,6-bis(1-methyl-1-phenylethyl)phenol (**HL$_3$**) were used as received, while 2-(2H-benzotriazol-2-yl)-6-dodecyl-4-methylphenol (**HL$_1$**) was purified by column chromatographically before use. The three new palladium(II) coordination compounds (Figure 1) were obtained by the complexation of the ligands with palladium(II) acetate in very good yields (>80%). The requirement of chromatographic purification is one reason for non-quantitative yields.

The ^{1}H NMR spectra of the free ligands (see Supporting Information) show the presence of a signal in the region 11.78 – 11.07 ppm which is attributed to the OH proton. The OH signal is not present in the spectra for the complexes supporting that the metal coordinates to the deprotonated oxygen-atom. A representative ^{1}H NMR spectrum for **PdL$_3$** is shown in Figure 2, highlighting the four signals of the inequivalent methyl groups. It is interesting to note that the ^{1}H NMR spectrum for **HL$_3$** displays two signals for the methyl groups. The aromatic region between 6 and 8 ppm is dominated by clear signals attributed to the benzotriazole: 11 signals are attributed to 32 protons, while in the aliphatic region 1–3 ppm are observed 5 different proton species: 4 signals are attributed to 24 protons from the methyl groups and the co-crystallized acetone peak.

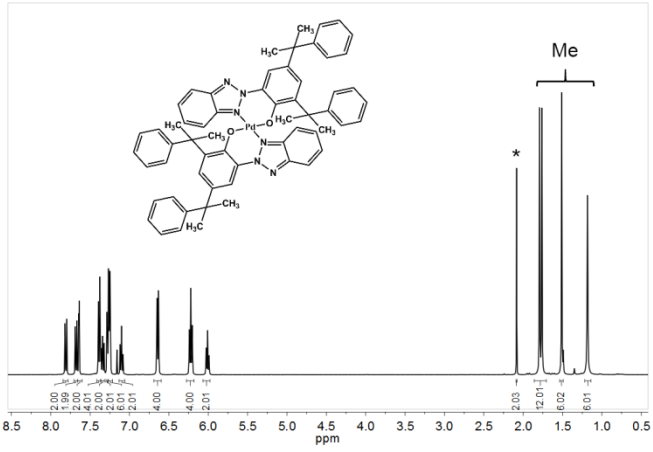

Figure 2. A 400 MHz ^{1}H NMR spectrum for **PdL$_3$** in $CDCl_3$ showing the four inequivalent methyl proton signals and the aromatic region. * = acetone.

Single crystal X-ray diffraction analysis

By using careful crystallization methods, a number of the products afforded crystals suitable for single-crystal X-ray diffraction analysis. Collected in Table S1 of Supporting Information are the relevant data for the structures **HL$_3$**, **PdL$_2$.H$_2$O**, **PdL$_3$**, and **PdL$_3$.(CH$_3$)$_2$CO**. The ligand **HL$_3$** crystallized in the monoclinic centrosymmetric space group P2/c with two independent molecules in the asymmetric unit, one of them showing some disorder at one phenyl site (two positions). The molecular structure of one molecule of **HL$_3$** is shown in Figure 3. All bond lengths and angles are within expected ranges. The hydroxyl group is intramolecular hydrogen bonded to one of the nitrogen atoms within the triazole unit to generate a six membered ring. The phenyl groups are positioned anti with respect to each other, although this is undoubtedly not the lowest energy arrangement; a basic MM$^+$ molecular mechanics calculation identified several close in energy conformations (see Supporting Information). The structure of **HL$_3$** also reveals the presence of intermolecular interactions within the crystal as at least four relevant π-stacking and five CH/π interactions can be reported (see Table S2 of Supporting Information).

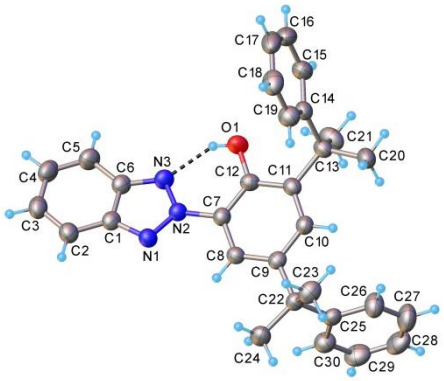

Figure 3. Single crystal X-ray diffraction determined molecular structure for **HL_3** drawn at 40% probability level showing the intramolecular hydrogen bond.

The molecular structure for the palladium complex with two **L3** ligands is illustrated in Figure 4. Complex **PdL_3** crystallized in the P21/c space group. The coordination mode at the palladium ion is a slightly distorted square planar arrangement, so that oxygen atoms of the hydroxyl are positioned trans, with the same arrangement observed for the nitrogen atoms of the triazole moieties. The N4-Pd1-N1 and O1-Pd1-O2 bond angles are 170.91(9) and 176.14(8), respectively. The Pd1-N1 and Pd1-N4 bond lengths of 2.001(2) Å and 2.013(2) Å are as expected. The Pd1-O1 and Pd1-O2 bond lengths of 1.995(2) Å and 1.999(2) Å are not within the standard deviation error different from the Pd-N bond lengths. Unlike the ligand alone, the complex is stabilized by two pairs of intramolecular π-stacking interactions between the benzotriazoles and two phenyl groups: the distances between centroids of rings N1/N2/N3/C60/C55 and C8/C9/C10/C11/C12/C13 and between centroids of rings N4/N5/N6/C30/C25 and C38/C39/C40/C41/C42/C43 are equal to 3.5566(18) Å and 3.572(2) Å, respectively, while the dihedral angles between these pairs of rings are equal to 1.28(16)° and 6.01(18)°, respectively. Thus, the complex adopts a rooftop conformation with one side of the Pd plane fully accessible, while the other side is partially protected by the two phenyl cycles involved in the π-stacking interactions (Figure 4).

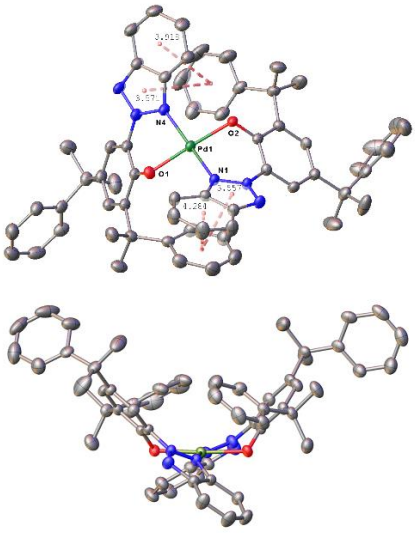

Figure 4. Single crystal X-ray diffraction determined molecular structure for **PdL_3** drawn at as 40% probability level ellipsoids showing selected labelling of atoms and distances in Å (top) and a view down the N4-Pd1-N1 axis (bottom).

Compound **$PdL_3.(CH_3)_2CO$** crystallized in the C2/c space group with two independent molecules in the asymmetric unit (see Supporting Information). The Pd atoms reside on the 2-fold axis and their coordination sphere is identical to that of complex **PdL_3**. Indeed the geometrical features observed in **$PdL_3.CH_3CO$** are comparable to those observed in **PdL_3**, with two pairs of intramolecular π-stacking interactions between the benzotriazoles and two phenyl groups, but the accessible sides of the Pd planes are now facing each other thus forming a pseudo dimer with the Pd1-Pd2 distance close to 4.2 Å.

Compound **$PdL_2.H_2O$** crystallized in the P21/n space group with two independent molecules in the asymmetric unit. The asymmetric unit (see Supporting Information) comprises one palladium(II) atom surrounded by two molecules of deprotonated **L_2** ligand, coordinated to the metal through two nitrogen and two oxygen atoms. The carbon atoms of the methyl and ethyl groups are partially delocalized and the structure contains a delocalized co-crystallised half water molecule.

Theoretical calculations

To elucidate both their structural and electronic features, the neutral, monoreduced and monooxidized complexes were subjected to DFT geometry optimizations (Figure 5A-C). Comparison of the DFT-optimized structure of **PdL_3** with the crystallographic one showed a pretty good agreement between the two sets of data, which confirmed that **PdL_3** can be best described as a diamagnetic square planar Pd(II) complex (**PdL_3**, S = 0). Whereas the Highest Occupied Molecular

Orbital (HOMO) for **PdL$_3$** resides on the ligand, the Lowest Unoccupied Molecular Orbital (LUMO) is very much centred on the palladium metal (Figure 6A-B), and is identified as the 4dx^2-y^2 orbital which is classically the unoccupied frontier orbital for a square planar complex. The mono-reduced **PdL$_3$** complex is best described as a Pd(I) paramagnetic species, S = ½, because of the elongation of the Pd-N and Pd-O bond lengths which supports that reduction occurs at the metal centre consistent with a Single Occupied Molecular Orbital (SOMO) being mainly distributed over the Pd centre and its coordinating atoms (Figure 6C). In the case of the mono-oxidized **PdL$_3$** complex it would appear that removal of an electron occurs at the ligand since the computed C-O and C-C bond lengths of the phenolate groups are affected. The species produced is therefore best described as paramagnetic Pd(II)-ligand radical species (S = ½) which is attested by the composition of the SOMO of the system (Figure 6D).

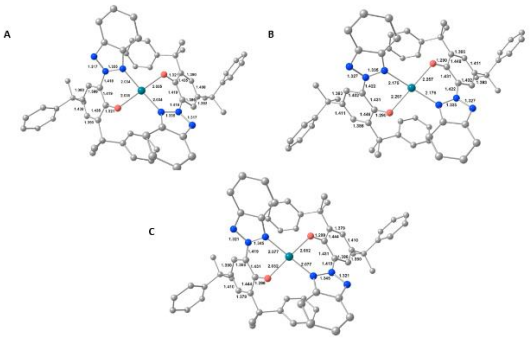

Figure 5. DFT-optimized structures of the neutral **PdL$_3$** complex (A), the mono-reduced **PdL$_3$** complex (B) and the one-electron oxidized **PdL$_3$** complex (C). Hydrogen atoms were omitted for clarity.

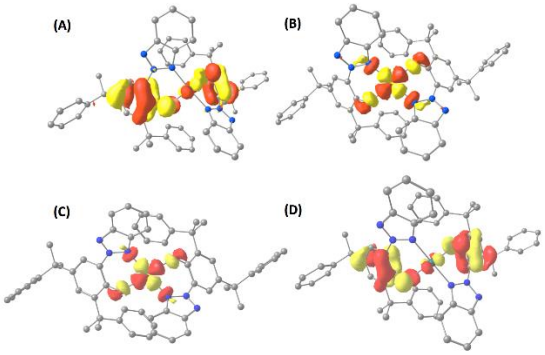

Figure 6. DFT-computed HOMO (A) and LUMO (B) for the neutral **PdL$_3$** complex, SOMO for the mono-reduced **PdL$_3$** (C) and SOMO for the one-electron oxidized **PdL$_3$** (D). Hydrogen atoms were omitted for clarity.

Cyclic voltammetry

The redox behaviour of the ligands **HL$_1$**, **HL$_2$**, **HL$_3$** (Figure 7, Table 1) were studied by cyclic voltammetry in dried DMF at a glassy-carbon electrode using 0.1 M *tetra*-Butylammonium PF_6 ($TBAPF_6$) as the supporting electrolyte. All potentials are referenced to the Fc^+/Fc redox couple. The redox behaviour for the ligands (Figure 7) is relatively straightforward and similar. The cathodic part of the CV is dominated by a quasi-reversible redox signal with $E_{1/2}^0$ = -2.20 V, -2.22 V, -2.15 V for **HL$_1$**, **HL$_2$**, **HL$_3$**, respectively. In the anodic region an irreversible signal is observed at $E_p^{a,1}$ = 0.80 V, 0.90 V, 0.95 V for **HL$_1$**, **HL$_2$**, **HL$_3$**, respectively.

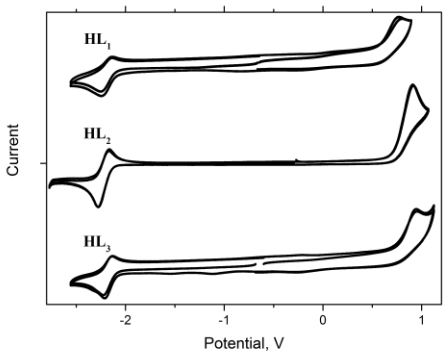

Figure 7. Cyclic voltammogram recorded for **HL$_1$**, **HL$_2$** and **HL$_3$** in N_2-purged DMF containing 0.1M $TBAPF_6$ vs Fc^+/Fc at a glassy carbon working electrode.

The redox behaviour of the complexes **PdL$_1$**, **PdL$_2$** and **PdL$_3$** (Figure 8, Table 1, Table S6) were studied by cyclic voltammetry in dried DMF at a glassy-carbon electrode using 0.1 M $TBAPF_6$ as the supporting electrolyte. All potentials are referenced to the Fc^+/Fe redox couple. There are clear similarities in the cyclic voltammograms for all three complexes. Upon oxidative scanning two clear irreversible waves are observed, which by comparison to the CVs of Figure 7, are ligand-based oxidations. The presence of two clear peaks is interpreted as oxidation at one ligand site affects the oxidation of the second ligand presumably by electronic communication via the Pd centre. The reduction side of the voltammograms are more interesting since they display a new wave at *ca.* – 1.5 V and are associated with the redox process at the metal site (Pd^{2+}/Pd^+). By increasing the potential window an additional irreversible wave is observed at a potential that is very close to the ligand-based redox process (*cf*. Figure 7). There is presumably some degradation process since upon reversing the scan an additional wave is observed at around -0.3 V. More breakdown products are evident when the potential scanning window is increased further, arising from the additional irreversible wave at *ca.* -2.9 V.

Table 1. CV data containing the half-wave potential of the first reduction process for complexes.[a]

	$E_{1/2}^2$
PdL$_1$	-1.57
PdL$_2$	-1.51
PdL$_3$	-1.59

[a] Data collected in dry DMF (0.1 M $TBAPF_6$) and referenced to Fc^+/Fc.

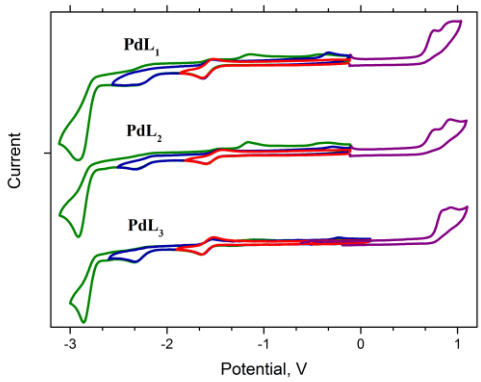

Figure 8. Cyclic voltammograms recorded for **PdL_1**, **PdL_2** and **PdL_3** in N_2-purged DMF containing 0.1M $TBAPF_6$ vs Fc^+/Fc at a glassy carbon working electrode over different potential ranges both in the reduction mode (red, blue and green lines) and in oxidation mode (purple lines).

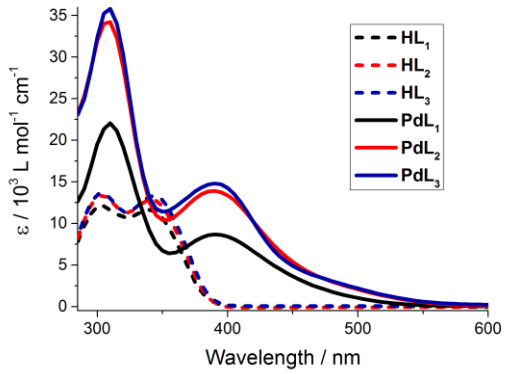

Figure 9. Electronic absorption spectra for ligands **HL_1**, **HL_2** and **HL_3** and for complexes **PdL_1**, **PdL_2** and **PdL_3** in DMF.

UV-Visible absorption spectroscopy

The room temperature electronic absorption spectra recorded for **HL_1**, **HL_2** and **HL_3** in DMF show two broad bands with absorption maxima λ_{max} at 305 and 340 nm for **HL_1** and **HL_2** and with λ_{max} at 305 and 345 nm for **HL_3** (Figure 9), and the relevant parameters are summarized in Table S6 of Supporting Information. In addition to ligand-based electronic transitions the absorption spectra recorded for **PdL_1**, **PdL_2** and **PdL_3** in DMF also show two broad bands with absorption maxima λ_{max} at 390 nm for **PdL_1** and **PdL_2** and with λ_{max} at 395 nm for **PdL_3** (Figure 9). For the complexes we also observe a minor shift for the first transition from 305 to 310 nm. The second electronic transition present for the ligands at 340-350 nm is absent for the case of the palladium complexes. This observation would suggest that the transition is associated with the hydroxyl group and likely of n-$\pi*$ character. The new band which appears at around 390 nm is related to the coordination of the ligand to the palladium and is of ligand-to metal charge transfer (LMCT) character.

The addition of up to 100 equivalents of TFA or acetic acid to a solution of **PdL_3** in DMF did not result in any significant changes to the absorption profile. There is a decrease in intensity and change in shape of the absorption band located at 390 nm upon formation of the mono-reduced species as expected since the LMCT transition is altered slightly. This new band does not change significantly in the presence of excess TFA. It would appear that the complex and its mono-reduced form are stable in the presence of excess acid (see Supporting Information).

Electrocatalysis

Given the behaviour of the complexes upon reduction we were interested to see if they also presented an electrocatalytic activity and were able to drive hydrogen production. The addition of either trifluoroacetic acid or acetic acid as a proton source to complexes **PdL_1**, **PdL_2** and **PdL_3** resulted in the formation of catalytic waves in the cathodic region of the cyclic voltammograms (see Supporting Information). A typical experiment is shown in Figure 10 for **PdL_3**. By using the "first derivative technique" the number and potential of the formed waves was estimated. For complex **PdL_3** three distinct waves were observed at -1.1 V, -1.6 V and -1.8 V, respectively. The current response increased with the addition of acid and the maximum for the peak shifted from -1.5 V to -1.9 V vs. Fc^+/Fc.

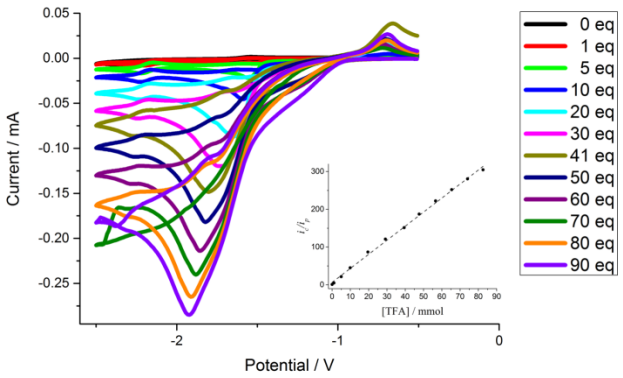

Figure 10. Selected cyclic voltammograms for **PdL_3** (1 mM) at a glassy carbon electrode in dry DMF in the presence of increasing quantities of TFA. Conditions: T = 298 K, scan rate 100 mV/s, supporting electrolyte: 0.1M $TBAPF_6$.

Gas analysis

A continuous flow-rig with in-line GC analysis was used to detect the molecular hydrogen produced during electrocatalytic proton reduction using **PdL_3** in DMF in the presence of TFA.[13] Applying a potential of -0.36 V vs NHE to a boron-doped diamond working electrode resulted in detection of molecular hydrogen (Figure 11). The rate of H_2 produced was determined by calibration with a known flow rate

of a H_2/Ar mixture, by checking the proportionality between the peak area and the volume of injected hydrogen per minute. When no complex was employed no hydrogen was detected during five hours of electrolysis. The presence of 1 mM of **PdL_3** resulted in three orders of magnitude increase of current at the same applied potential and immediate constant production of hydrogen as indicated by the GC analysis. Almost seven turnovers were reached after five hours of electrolysis and no sign of hydrogen production decrease was observed at the end of this time. At the same time a low constant faradaic yield of about 50 % was noticed. The UV-Vis spectrum and the cyclic voltammogram of the electrolysis solution did not change significantly during electrolysis. This would suggest that the low faradaic yield of the detected hydrogen is more likely to be a result of substrate reduction. Palladium complexes are well known catalysts for chemical and electrochemical hydrogenation of organic compounds.[14] As the produced hydrogen cannot be removed immediately from the solution hydrogenation of the electrolysis mixture components is quite likely.

Interestingly, after performing similar gas analysis experiments using a working mercury pool electrode no gaseous hydrogen formation was observed. This finding does suggest that the molecular complex is not the active catalyst, and that it is more likely a precursor for generation of the catalytic species. The simplest answer is metallic palladium formation upon reduction of Pd(II) to Pd(0) in the complex accompanied by loss of the ligands. As most of the Pd complex seems to be still present in solution after electrolysis, most likely only a small percentage of **PdL_3** is initially converted to metallic Pd and is responsible for the electrocatalysis. The reductive hydrogenation of the free ligand seems to be the most likely candidate to compete with hydrogen production.

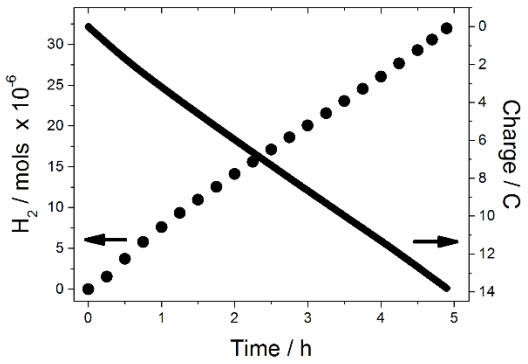

Figure 11. Electrocatalytic hydrogen production vs. time and charge vs. time by applying -0.36 V vs. NHE to a glassy carbon electrode in 0.1 M $TBAPF_6$ solution of DMF containing 90 mM TFA and 1 mM **PdL_3** complex.

Sonogashira and Heck C-C cross couplings

The industrially important Sonogashira Pd-catalysed C-C coupling of a sp-hybridized carbon from a terminal alkyne with a sp^2-hybridized carbon from an aryl halide to afford a substituted acetylene traditionally requires the presence of a copper co-catalyst which brings some problems (e.g., competitive homocoupling to the diyne) to the catalytic system.[15,16] To address such issues, copper-free synthetic strategies are in high demand. Herein, the Cu-free Sonogashira C-C cross coupling of phenylacetylene and iodobenzene (as a model reaction) was attempted in the presence of **PdL_2** or **PdL_3**, under microwave (MW) irradiation (Figure 12a). At room temperature no C-C coupling products were detected, therefore MW irradiation was the chosen (green) heating mode. In order to probe the synthetic scope of this Cu-free Pd-catalysed MW-assisted Sonogashira-type reaction, experimental conditions were optimized by using different bases, solvents, as well as MW power and reaction temperatures, and the results for the best combinations are presented in Table 2.

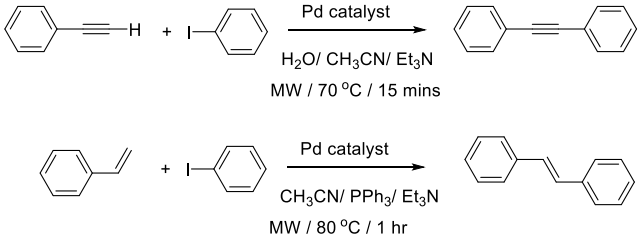

Figure 12. Microwave (MW) assisted a) Sonogashira C-C cross-coupling reaction of phenylacetylene and iodobenzene or b) Heck C-C cross-coupling between styrene and iodobenzene, catalysed by **PdL_2** or **PdL_3**.

Table 2. Selected results from the MW-assisted Cu-free cross-coupling of iodobenzene with phenylacetylene catalysed by **PdL_2** or **PdL_3**.[a]

Entry	Catalyst	T °C	Base	Solvent	Time mins	Yield[b] %	TON 10^3 [c]
1		50	Et_3N	DCM	15	75	7.5
2	**PdL_2**	90	K_2CO_3	DMF	30	79	7.9
3		70	Et_3N	MeCN/ H_2O	15	87	8.7
4		50	Et_3N	DCM	15	73	7.3
5	**PdL_3**	90	K_2CO_3	DMF	30	76	7.6
6		70	Et_3N	MeCN/ H_2O	15	84	8.4
7	**$Pd(OAc)_2$**	70	Et_3N	MeCN/ H_2O	15	40	4.0

[a] Reaction conditions: Pd-catalyst (0.01 mmol), iodobenzene (1 mmol), phenylacetylene (1.1 mmol), base (1.2 mmol), solvent (3 mL), MW (50 W). [b] Isolated yield. [c] TON (Turnover number) = moles of product per mol of catalyst.

As seen from the data in Table 2 very similar results for both compounds were obtained, leading to maximum yields of 87% and 84% of diphenylacetylene for the Pd-complexes **PdL_2** and

PdL₃, respectively, after 15 mins of MW irradiation at 70 °C in an acetonitrile/water medium. The catalytic activity of complexes **PdL₂** and **PdL₃** was also tested for the versatile and industrially important[17–19] Csp^2-Csp^2 coupling of organic halides with olefins (Heck reaction). The selected halide substrates were styrene and iodobenzene. The reaction was performed according to Figure 12b using triphenylphosphine as the reducing agent, in the presence of triethylamine, in a sealed reactor and under microwave irradiation, typically at 80 °C. In all Heck experiments, the selectivity for trans-stilbene was 100% (the only product detected). After 1 h of MW irradiation (90 W power) at 80 °C under optimized conditions, similar yields, 91% and 88%, respectively, of trans-stilbene were obtained in the presence of **PdL₂** and **PdL₃**.

It is worth noting that for both Sonogashira and Heck C-C cross couplings, the catalytic performance of **PdL₂** and **PdL₃** was clearly superior to that exhibited by their Pd precursor, $Pd(OAc)_2$. As presented in Table 2 (entry 7) for the Sonogashira reaction, the coupling product maximum yield of 40% was obtained when $Pd(OAc)_2$ was used as catalyst. In addition, the Heck reaction carried out in the presence of $Pd(OAc)_2$ led only to 54% of trans-stilbene. The coordination sphere at the palladium metal for **PdL₂** and **PdL₃** during the catalytic cycle is evidently disposed to facilitate the stereoselective reaction. Noting that the molecular structure of **PdL₃** does show that one face of the complex is hindered by the phenyl groups, this feature may play a significant role in controlling the reductive elimination step.

Conclusions

Neutral lipophilic palladium complexes are readily prepared through the employment of cheap and readily available organic benzotriazolyl phenolate precursors. The complexes show limited capabilities as electrocatalytic hydrogen producers, since it appears that they decompose during repeating cycling, likely forming metallic palladium particles. Nevertheless, they are more productive in C-C coupling reactions outperforming the simple neutral complex $Pd(OAc)_2$ in Sonogashira and Heck reactions. The lipophilic nature of the complexes does open up the opportunity to possibly perform cross-coupling reactions in more controlled environments such as oil droplets or emulsions that have application in flow chemistry.[20] In addition, the basic ligand structure is also set up for the addition of other functionality. For example, the R_1 and R_2 groups (Figure 1) could readily contain sites for attachment to surfaces, polymers and beads to support heterogeneous coupling reactions. Future work is intended to explore the development of the ligands along the outlined lines.

Experimental Section

All chemicals were purchased from commercial sources and used as received unless otherwise stated. Basic solvents for synthesis were dried using literature methods. Solvents for spectroscopic investigations were of the highest purity available.

Electrochemical investigations were carried out on Pd incorporated complexes in DMF/n-NBu_4PF_6 (0.1 M) solution at ambient temperature using a three-electrode configuration (glassy carbon working electrode, Pt counter electrode, $Ag/AgNO_3$ reference). All potentials are presented vs Fc^+/Fc redox couple. Gaseous H_2 detection was performed using the method described by Summers *et al.*[13] 1 mM solutions of catalyst in DMF containing TFA (90 mM) and $TBAPF_6$ (0.1 M) were prepared from thoroughly degassed stock solutions and stored under argon. Argon gas was continually flowed through the solution and into a 6-port 2-position switch (VICI) at a constant flow (10 mL min^{-1}), which was maintained using a mass flow controller (Bronkhorst, E-Flow series). A 200 µL sample was analysed automatically every 3.2 mins using a gas chromatograph (Shimadzu GC2014) with a thermal conductivity detector operating at 50 °C. The sample was initially passed through a dry ice trap to remove any condensable solvents. Argon was used as the carrier gas and H_2 was detected on an activated molecular sieve column (Shincarbon ST, Restek). Integration of a plot of the production rate versus time yielded the total amount of H_2 produced. A voltage was applied using an IVIUMSTAT potentiostat, a boron doped diamond working electrode, platinum mesh counter electrode, $Ag/AgNO_3$ (0.01 M) reference electrode were employed and the potentials were converted to the NHE scale by adding 0.54 V.[21]

Elemental analyses were performed using a Thermo Finnigan EA 1112 instrument. The results were validated by at least two measurements. UV-Vis spectra were recorded on a Varian Cary 50 spectrophotometer from 200-800 nm with samples in a 1.0 cm pathlength quartz cuvette. FT-IR spectra were recorded in attenuated total reflection (ATR) mode on a Bruker TENSOR 27 spectrometer equipped with a single-reflection DuraSamplIR diamond ATR accessory. Intensities are mentioned in the parenthesis as vs = very strong, s = strong, m = medium, w = weak, vw = very weak and sh = shoulder. NMR spectra were recorded on a BruckerAvance III nanobay spectrometer (300 or 400 MHz) using TMS as internal reference. ESI-MS analyses were performed using a SYNAPT G2 HDMS (Waters) spectrometer equipped with a pneumatically assisted Atmospheric Pressure Ionization (API) source. The ion-spray voltage was 2.8 kV, the orifice lens was 20 V, and the nitrogen flux (nebulization) was 100 L h^{-1}. The HR mass spectra were obtained with a time-of-flight (TOF) analyzer. The sample was placed in a methanol/3mM ammonium acetate.

Synthesis of bis[2-(2H-benzotriazol-2-yl)-6-dodecyl-4-methylphenolato]palladium(II) (PdL_1)

To a solution of 2-(2H-benzotriazol-2-yl)-6-dodecyl-4-methylphenol (**HL_1**) (0.25 g, 0.6 mmol) in THF (3 mL) at ambient temperature was added dropwise a solution of $Pd(OAc)_2$ (0.07 g, 0.3 mmol) in THF (4 mL). The obtained orange mixture with

the total volume of 7 mL was stirred at 20 °C. The reaction was monitored by TLC. After 48 h volatile materials were removed under vacuum. The oily product obtained was purified by flash chromatography on silica gel using the eluent petroleum ether/methylene chloride (99:1). Compound **PdL_1** was isolated as an orange oily product. Yield: 0.2325 g, 83.7%. IR, ν (cm^{-1}) = 2954.9 (m), 2922.1 (s), 2852.7 (m), 1608.6 (w), 1572.0 (w), 1556.5 (w), 1490.9 (m), 1465.9 (s), 1411.9 (w), 1377.1 (w), 1352.1 (m), 1342.4 (m), 1307.7 (m), 1288.4 (m), 1244.1 (s), 1203.6 (m), 1149.6 (m), 1134.1 (w), 1114.8 (w), 1078.2 (w), 1037.7 (w), 987.5 (w), 976.0 (w), 947.0 (w), 906.5 (m), 856.4 (m), 819.7 (m), 763.8 (m), 734.9 (vs), 680.9 (w), 648.1 (w), 636.5 (w), 557.4 (m), 511.1 (w), 443.6 (w). ^{1}H-NMR (400 MHz, $CDCl_3$, ppm): δ 8.48 (broad singlet, 2H, CH), 8.00 (d, 2H, *J* = 9.0 Hz, CH), 7.59 (s, 2H, CH), 7.55 (t, 4H, *J* = 6.5Hz CH,), 6.81 (s, 2H, CH), 2.26 (s, 6H, CH, CH_3-methyl), 1.22 (t, 6H, *J* = 7.0 Hz, CH, CH_3-dodecyl), 0.86 (m, 44H, CH, CH_2-dodecyl). ESI-MS (DCM): m/z 891.45 $[M+H]^+$. UV-Vis (DMF): λ_{max}, nm (ε, 10^3 L mol^{-1} cm^{-1}): 310 (22.0), 390 (8.6).

Synthesis of bis[2-(2H-Benzotriazol-2-yl)-4,6-di-tert-pentylphenolato]palladium(II) (PdL_2)

To a solution of 2-(2H-benzotriazol-2-yl)-4,6-di-tert-pentylphenol (**HL_2**) (0.70 g, 2.0 mmol) in THF (10 mL) at ambient temperature was added dropwise a solution of $Pd(OAc)_2$ (0.22 g, 1.0 mmol) in THF (15 mL). The obtained dark red mixture with the total volume of 25 mL was stirred at 20 °C. The reaction was monitored by TLC. After 48 h volatile materials were removed under vacuum. The product obtained was purified by flash chromatography on silica gel using the eluent petroleum ether/methylene chloride (99:1). Compound **PdL_2** was isolated as an orange solid. Yield: 0.7309 g, 92.4 %. Suitable crystals for single crystal X-ray diffraction study of (**$PdL_2.H2O$**) were grown by recrystallization from chloroform. Elemental Anal.: Calcd.: C, 65.46; H, 6.99; N, 10.41; ($C_{44}H_{56}N_6O_2Pd$); Found: C, 65.66; H, 6.95; N, 10.15 %. IR, ν (cm^{-1}) = 2960.7 (m), 2910.5 (w), 2873.9 (w), 1573.9 (w), 1460.1 (m), 1440.8 (m), 1404.1 (m), 1381.0 (w), 1352.1 (w), 1328.9 (w), 1309.6 (m), 1282.6 (m), 1244.1 (m), 1228.6 (m), 1199.7 (w), 1166.9 (w), 1149.6 (w), 1137.97 (w), 1111.0 (w), 1057.0 (w), 1006.8 (w), 987.5 (w), 974.0 (vw), 939.3 (w), 896.9 (vw), 871.8 (w), 840.9 (vw), 825.5 (w), 808.2 (w), 781.2 (w), 763.8 (w), 740.7 (vs), 723.3 (m), 690.5 (w), 663.5 (w), 638.4 (w), 592.1 (w), 563.2 (m), 538.1 (w), 516.9 (m), 505.3 (w), 474.5 (w), 441.7 (m), 395.4 (w), 356.8 (w), 314.4 (m). ^{1}H-NMR (400 MHz, $CDCl_3$): δ 8.34 (d, 2H, *J* = 8.3 Hz CH), 8.04 (d, 2H, *J* = 6.7 Hz CH), 7.78 (s, 2H, CH), 7.58 (t, 4H, *J* = 9.3 Hz CH), 7.19 (s, 2H, CH), 1.69 (d, 8H, *J* = 8.7 Hz CH_2-ethyl), 1.34 (s, 12H, CH_3-methyl), 1.16 (s, 6H, CH_3-methyl), 1.00 (s, 6H, CH_3-methyl), 0.81 (t, 6H, *J* = 7.3 Hz CH_3-ethyl), 0.45 (t, 6H, *J* = 7.9 Hz CH_3-ethyl). ESI-MS (DCM): m/z 807.36 $[M+H]^+$. UV-Vis (DMF): λ_{max}, nm (ε, 10^3 L mol^{-1} cm^{-1}): 310 (34.2), 390 (13.9).

Synthesis of bis[2-(2H-Benzotriazol-2-yl)-4,6-bis(1-methyl-1-phenylethyl)phenolato]palladium(II) (PdL_3)

To a solution of 2-(2H-benzotriazol-2-yl)-4,6-bis(1-methyl-1-phenylethyl)phenol (**HL_3**) (0.90 g, 2.0 mmol) in THF (10 mL) at ambient temperature was added dropwise a solution of $Pd(OAc)_2$ (0.22 g, 1.0 mmol) in THF (15 mL). The obtained deep red mixture with the total volume of 25 mL was stirred at 20 °C. The reaction was monitored by TLC. After 48 h volatile materials were removed under vacuum. The obtained product was purified by flash chromatography on silica gel using the eluent petroleum ether/methylene chloride (99:1). Compound **PdL_3** was isolated as an orange solid. Yield: 0.9165 g (93.95 %. Suitable crystals for single crystal X-ray diffraction study of (**PdL_3**) were grown by recrystallization from DMF (orange hexagons). Elemental Anal.: Calcd.: C, 72.10; H, 5.65; N, 8.41; ($C_{60}H_{56}N_6O_2Pd$); Found: C, 72.17; H, 5.57; N, 8.28 %. IR, ν (cm^{-1}) = 2964.5 (w), 2933.7 (w), 2868.1 (w), 1597.0 (w), 1492.9 (w), 1462.0 (m), 1440.8 (m), 1408.0 (m), 1384.9 (w), 1354.0 (w), 1311.6 (m), 1288.4 (m), 1251.8 (m), 1230.6 (m), 1220.9 (m), 1188.1 (w), 1145.7 (w), 1128.3 (w), 1107.1 (w), 1072.4 (w), 1030.0 (w), 987.5 (w), 933.5 (w), 896.9 (w), 873.7 (w), 856.4 (w), 815.9 (m), 761.9 (s), 748.4 (s), 715.6 (w), 696.3 (vs), 667.4 (w), 650.0 (m), 636.5 (w), 615.3 (w), 605.6 (m), 578.6 (w), 561.3 (m), 551.6 (m), 528.48 (w), 509.2 (w), 497.6 (m), 472.6 (w), 455.2 (m), 443.6 (m), 410.8 (m), 403.1 (m), 383.8 (w), 366.5 (w), 326.0 (m). ^{1}H-NMR (400 MHz, $CDCl_3$, ppm): δ 7.82 (d, 2H, *J* = 8.7 Hz CH), 7.67 (d, 2H, *J* = 8.7 Hz), 7.64 (s, 2H, CH), 7.39 (d, 4H, *J* = 7.4 Hz CH,), 7.36 (t, 2H, *J* = 7.6 Hz CH,) 7.29 (s, 2H, CH), 7.27 (d, 6H, *J* = 8.2 Hz, CH), 7.12 (t, 2H, *J* = 7.6 Hz, CH,) 6.65 (d, 4H, *J* = 7.7 Hz CH), 6.24 (t, 4H, *J* = 7.4 Hz CH), 6.03 (t, 2H, *J* = 7.4 Hz CH), 1.79 (s, 6H, CH_3), 1.76 (s, 6H, CH_3), 1.51 (s, 6H, CH_3), 1.18 (s, 6H, CH_3). ESI-MS (DCM): m/z 999.36 $[M+H]^+$. UV-Vis (DMF): λ_{max}, nm (ε, 10^3 L mol^{-1} cm^{-1}): 310 (35.8), 390 (14.8). Recrystallization of (**PdL_3**) from acetone gave the compound (**$PdL_3.(CH_3)_2CO$**). Orange needles. For $[Pd(C_{30}H_{28}N_3O)_2 \cdot 0.5(CH_3)_2CO]$: Elemental Anal.: Calcd.: C, 71.81; H, 5.78; N, 8.17; ($C_{61.5}H_{59}N_6O_{2.5}Pd$); Found: C, 71.90; H, 5.61; N, 8.10 %.

Single crystal X-ray diffraction analysis

The intensity data for compounds **HL_3**, **PdL_3** and **$PdL_3.(CH_3)_2CO$** were collected on a Rigaku Oxford Diffraction SuperNova diffractometer and on a Rigaku Oxford Diffraction Xcalibur, Eos diffractometer for **$PdL_2.H_2O$** using CuK_α radiation (λ = 1.54184 Å) for the ligand **HL_3** and MoK_α radiation (λ = 0.71073 Å) for the Pd complexes. Data collection, cell refinement and data reduction were performed with CrysAlisPro (Rigaku Oxford Diffraction), the structure were solved with SIR92[22] or SHELXS[23] and SHELXL-2013[23] was used for full matrix least squares refinement. The hydrogen atoms were found experimentally for compounds **HL_3** and **PdL_3**, except for the disordered phenyl for **HL_3** were they were introduced at geometrical positions. For compounds **$PdL_3.(CH_3)_2CO$** and **$PdL_2.H_2O$** the H-atoms were all introduced at geometrical positions. For each structure the hydrogen atoms were refined as riding atoms with their Uiso parameters fixed to 1.2Ueq (parent atom) for the aromatics carbons and to 1.5Ueq (parent atom) for the remaining atoms.

CCDC 1965954 (for **HL_3**), 1966865 (for **$PdL_2.H_2O$**), 1965953 (for **PdL_3**) and 1965955 (for **$PdL_3.(CH_3)_2CO$**) contain the

supplementary crystallographic data for this paper. These data can be obtained free of charge from The Cambridge Crystallographic Data Centre.

DFT calculations

All theoretical calculations were performed with the ORCA program package.[24] Full geometry optimizations and signle point calculations were carried out using the hybrid functional B3LYP[25,26] in combination with the TZV/P[27] basis set for all atoms and by taking advantage of the resolution of the identity (RI) approximation in the Split-RI-J variant[28] with the appropriate Coulomb fitting sets.[29] Increased integration grids (Grid4 in ORCA convention) and tight SCF convergence criteria were used. Solvent effects were accounted for according to the experimental conditions. For that purpose, we used the DMF (ε = 38.3) solvent within the framework of the conductor like screening (COSMO) dielectric continuum approach.[30] Molecular orbitals were generated using the orca plot utility program and were visualized with the Chemcraft program.[31]

The microwave-assisted C-C cross coupling reactions were performed in G10 borosilicate glass tubes (10 mL capacity reaction tube with a 13 mm internal diameter) in a focused Anton Paar Monowave 300 reactor fitted with a rotational system and an IR temperature detector.

Sonogashira C-C coupling

The desired amount of catalyst (0.001-0.010 mmol), phenylacetylene (1.0 mmol), iodobenzene (1.1 mmol), Et_3N (1.2-3.0 mmol) and the solvent (3.0 mL) were introduced into the Pyrex tube, closed, placed in the microwave reactor and maintained under stirring and under low power (10-100 W) irradiation for the desired temperature and reaction time. After the reaction, the obtained mixture was cooled to room temperature, the organics extracted with diethyl ether (5.0 mL) and the 1,2-diphenylethyne isolated and spectroscopically characterized. Control experiments were performed under the optimized reaction conditions but in the presence of $Pd(OAc)_2$ instead of any complex catalyst. Blank experiments (without a metal catalyst) were performed and no C-C coupling products were detected. In addition, a mercury drop experiment was performed by adding two drops of metallic Hg to the abovementioned reaction mixture and running the reaction under the optimized reaction conditions. After the reaction, the obtained mixture was cooled to room temperature, filtered, and treated and analysed as above. No significant difference in conversion was observed.

Heck C-C coupling

*T*he desired amount of catalyst (0.001-0.010 mmol), styrene (2.0 mmol), iodobenzene (1.0 mmol), PPh_3 (0.05-0.10 mmol), Et_3N (1.0-2.0 mmol) and acetonitrile (2.5 mL) were introduced into the Pyrex tube, closed, placed in the microwave reactor and maintained under stirring and under low power (50-150 W) irradiation for the desired temperature and reaction time. After the reaction, the obtained mixture was cooled to room temperature, the organics extracted with diethyl ether (5.0 mL) and evaporated to dryness under a stream of dinitrogen. Then, the residue was dissolved in $CDCl_3$ and analysed by ^1H NMR at Bruker 300 and 400 UltraShield™ spectrometers. The yield of C-C coupling product (relatively to iodobenzene) was established using an internal standard.[32] Control experiments were performed under the same reaction conditions but in the presence of $Pd(OAc)_2$ instead of any complex catalyst. Blank experiments (without a metal catalyst) were performed and no C-C coupling products were detected. In addition, a mercury drop experiment was performed by adding two drops of metallic Hg to the abovementioned reaction mixture and running the reaction under the optimized reaction conditions. After the reaction, the obtained mixture was cooled to room temperature, filtered, and treated and analysed as above. No significant difference in conversion was observed.

Acknowledgments

Dr. Amélie Kochem is thanked for useful discussions and advice. This work has been partially supported by the Fundação para a Ciência e a Tecnologia (FCT), Portugal; projects UID/QUI/00100/2019 and PTDC/QEQ-ERQ/1648/2014 are acknowledged. Newcastle University is thanked for support to the project.

Keywords: Palladium complexes • Electrocatalysis • Heck • Sonogashira • X-ray structures

References

[1] M. Hartings, *Nat. Chem.,* **2012**, 4, 764–764.
[2] K. L. Walker, L. M. Dornan, R. N. Zare, R. M. Waymouth, M. J. Muldoon, *J. Am. Chem. Soc.,* **2017**, 139, 12495–12503.
[3] C. A. Sanz, Z. R. McKay, S. W. C. MacLean, B. O. Patrick, R. G. Hicks, *Dalton Trans.,* **2017**, 46, 12636–12644.
[4] J. N. Butler, A. C. Makrides, *Trans. Faraday Soc.,* **1964**, 60, 938-946.
[5] J. Chu, X. Xie, S. Yang, S. Zhan, *Inorg. Chim. Acta,* **2014**, 410, 191–194.
[6] D. Sirbu, C. Turta, E. A. Gibson, A. C. Benniston, *Dalton Trans.,* **2015**, 44, 14646–14655.
[7] T. Straistari, R. Hardré, J. Massin, M. Attolini, B. Faure, M. Giorgi, M. Réglier, M. Orio, *Eur. J. Inorg. Chem.,* **2018**, 2259–2266.
[8] B. V. Zakharchenko, D. M. Khomenko, R. O. Doroshchuk, I. V. Raspertova, V. S. Starova, V. V. Trachevsky, S. Shova, O. V. Severynovska, L. M. D. R. S. Martins, A. J. L. Pombeiro, V. B. Arion, R. D. Lampeka, *New J. Chem.,* **2019**, 43, 10973–10984.
[9] H. V. Huynh, C.-S. Lee, *Dalton Trans.,* **2013**, 42, 6803-6809.
[10] E. Díez-Barra, J. Guerra, V. Hornillos, S. Merino, J. Tejeda, *Organometallics*, **2003**, 22, 4610–4612.
[11] Negishi, L. Anastasia, *Chem. Rev.,* **2003**, 103, 1979–2018.
[12] O. Cuzan, A. Kochem, A. J. Simaan, S. Bertaina, B. Faure, V. Robert, S. Shova, M. Giorgi, M. Maffei, M. Réglier, M. Orio, *Eur. J. Inorg. Chem.,* **2016**, 5575–5584.
[13] P. A. Summers, J. Dawson, F. Ghiotto, M. W. D. Hanson-Heine, K. Q. Vuong, E. Stephen Davies, X.-Z. Sun, N. A. Besley, J. McMaster, M. W. George, M. Schröder, *Inorg. Chem.* **2014**, 53, 4430–4439.
[14] A. Deronzier, J.-C. Moutet, E. Saint-Aman, *J.Electroanal. Chem.,* **1992**, 327, 147–158.
[15] K. Sonogashira, Y. Tohda, N. Hagihara, *Tetrahedron Lett.,* **1975**, 16, 4467–4470.
[16] K. Sonogashira, *J. Organometallic Chem.,* **2002**, 653, 46–49.
[17] I. P. Beletskaya, A. V. Cheprakov, *Chem. Rev.* **2000**, 100, 3009–3066.
[18] J. Magano, J. R. Dunetz, *Chem. Rev.,* **2011**, 111, 2177–2250.

[19] L. M. D. R. S. Martins, A. M. F. Phillips, A. J. L. Pombeiro, in Green Chemistry Series (Eds.: M.M. Pereira, M.J.F. Calvete), Royal Society Of Chemistry, Cambridge, 2018, pp. 193–229.
[20] V. Misuk, A. Mai, K. Giannopoulos, D. Karl, J. Heinrich, D. Rauber, H. Löwe, *J. Flow Chem.,* **2015**, 5, 43–47.
[21] R. A. Scott, C. M. Lukehart, Eds. , Applications of Physical Methods to Inorganic and Bioinorganic Chemistry, Wiley, Hoboken, NJ, 2007.
[22] A. Altomare, G. Cascarano, C. Giacovazzo, A. Guagliardi, M. C. Burla, G. Polidori, M. Camalli, *J. Appl. Crystallography*, **1994**, 27, 435–435.
[23] G. M. Sheldrick, *Acta Cryst. Section A Foundations of Crystallography* **2008**, 64, 112–122.
[24] F. Neese, *WIREs Comput. Mol. Sci.,* **2012**, 2, 73–78.
[25] A. D. Becke, *J. Chem. Phys.,* **1993**, 98, 1372–1377.
[26] C. Lee, W. Yang, R. G. Parr, *Phys. Rev. B*, **1988**, 37, 785–789.
[27] A. Schäfer, C. Huber, R. Ahlrichs, *J. Chem. Phys.,* **1994**, 100, 5829–5835.
[28] F. Neese, *J. Comput. Chem*., **2003**, 24, 1740–1747.
[29] F. Weigend, *Phys. Chem. Chem. Phys.,* **2006**, 8, 1057-1065.
[30] A. Klamt, G. Schüürmann, *J. Chem. Soc., Perkin Trans. 2*, **1993**, 799–805.
[31] Chemcraft - graphical software for visualization of quantum chemistry https://www.chemcraftprog.com.
[32] L. Xu, W. Chen, J. Xiao, *Organometallics*, **2000**, 19, 1123–1127.